Article

Hydrogen Bonding in Redox-Modulated Molecular Recognition. An Experimental and Theoretical Investigation

Mark Gray, Alejandro O. Cuello, Graeme Cooke, and Vincent M. Rotello

J. Am. Chem. Soc., **2003**, 125 (26), 7882-7888• DOI: 10.1021/ja035228b • Publication Date (Web): 10 June 2003

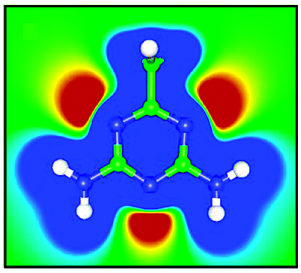

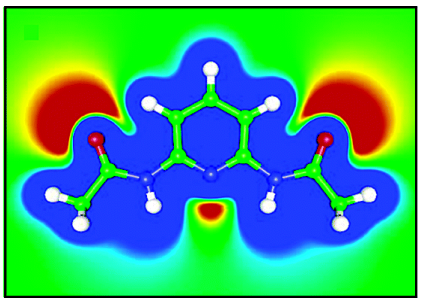

J|A|C|S
ARTICLES
Published on Web 06/10/2003

Hydrogen Bonding in Redox-Modulated Molecular Recognition. An Experimental and Theoretical Investigation

Mark Gray,[†] Alejandro O. Cuello,[†] Graeme Cooke,[‡] and Vincent M. Rotello*[,†]

Contribution from the Department of Chemistry, University of Massachusetts, Amherst, Massachusetts 01003, and Centre for Biomimetic Design and Synthesis, Department of Chemistry, Heriot-Watt University, Riccarton, Edinburgh, U.K. EH14 4AS

Received March 19, 2003; E-mail: rotello@chem.umass.edu

Abstract: Two receptors, a diaminotriazine derivative (**DAT**) and diamidopyridine (**DAP**), are complementary to the electroactive naphthalimide (**N**) through three-point hydrogen bonding. The association constants of the two receptors were evaluated for both the fully oxidized and the radical anion forms of **N**. In the oxidized state, the two receptors displayed identical binding constants. Diamidopyridine, however, lowers the reduction potential of naphthalimide to a far greater extent than does diaminotriazine, indicating a greater affinity for diamidopyridine by naphthalimide in the radical anion form. This behavior was mirrored by EPR experiments that showed small deviations from the hyperfine coupling pattern of $\mathbf{N_{red}}$ in the presence of **DAT**, with greater effects seen for the $\mathbf{N_{red}}$**·DAP** complex. Computational simulations using the UB3LYP/6-311+G-(d,p)//UHF/6-31G(d) hybrid gave theoretical hyperfine constants in good quantitative agreement with the experimental results. Using this correlation, we determined that electrostatics and hydrogen bond polarizability play key roles in controlling redox-modulated molecular recognition.

Introduction

Functional systems are created, modified, and fine-tuned in nature through noncovalent forces. One of these forces, hydrogen bonding, is central to a range of intra- and intermolecular phenomena in the natural world.[1] The strength and directionality of these interactions direct protein folding and stabilization, while the ability to encode information into hydrogen-bonded networks allows for the storage and transfer of genetic data from DNA.[2] Biological systems also use hydrogen bonding to stabilize specific oxidation states of pterins,[3] quinones,[4] nicotinamides,[5] and flavins[6] through specific interactions with a protein scaffold.

Many of the electroactive molecular devices in the forms of switches,[7] shuttles,[8] logic gates,[9] and sensors[10] that have been developed in recent years are inspired by the way functional natural systems utilize noncovalent interactions. In particular, hydrogen bonding has emerged as a powerful tool in the creation of device-oriented supramolecular ensembles.[11] Previously, we[12] and others[13] have studied the interplay between hydrogen bond formation and redox potential modulation of electroactive compounds both to gain a greater understanding of the underlying chemistry of these systems and to begin the rational design of the next generation of electroactive supramolecular device.[14]

In general, preferential hydrogen bonding to one oxidation state of a redox-active guest leads to efficient redox modulation. However, as in all intermolecular forces, several components participate in hydrogen bonding with significant contributions, including induction and dispersion forces as well as electrostatic events.[15] Several computational models have been proposed to probe the hydrogen-bonding interaction at the electronic level.[16] For biomolecular systems, hydrogen bonds are generally treated as being electrostatic in nature.[17] In a study performed on the interaction between water and a protein with charged residues, however, it was found that electrostatic interactions are less

[†] University of Massachusetts.
[‡] Heriot-Watt University.

(1) Jeffrey, G. A.; Saenger, W. *Hydrogen Bonding in Biological Structures*; Springer-Verlag: Berlin, 1991.
(2) Fersht, A. R. *Enzyme Structure and Mechanism*; W. H. Freeman & Co.: New York, 1985.
(3) Blakely, R. L.; Benkovic, S. J. *Chemistry and Biochemistry of Pterins*; Wiley: New York, 1985.
(4) Anthony, C. *Biochem. J.* **1996**, *320*, 697−711.
(5) Popov, V.; Lamzin, V. S. *Biochem. J.* **1994**, *301*, 625−643.
(6) Ghisla, S.; Massey, V. *Eur. J. Biochem.* **1989**, *181*, 1−17.
(7) Otsuki, J.; Tsujino, M.; Iizaki, T.; Araki, K.; Seno, M.; Takatera, K.; Watanabe, T. *J. Am. Chem. Soc.* **1997**, *119*, 7895−7896.
(8) Anelli, P. L.; Spencer, N.; Stoddart, J. F. *J. Am. Chem. Soc.* **1991**, *113*, 5131−5133.
(9) De Silva, A. P.; Gunaratne, H. Q. N.; McCoy, C. P. *J. Am. Chem. Soc.* **1997**, *119*, 7891−7892.
(10) Swager, T. M. *J. Am. Chem. Soc.* **1995**, *117*, 12593−12602.
(11) (a) Cooke, G.; Rotello, V. M. *Chem. Soc. Rev.* **2002**, *31*, 275−286. (b) Prins, L. J.; Reinhoudt, D.; Timmerman, P. *Angew. Chem., Int. Ed.* **2001**, *40*, 2382.
(12) Niemz, A.; Rotello, V. M. *Acc. Chem. Res.* **1999**, *32*, 44−52.
(13) (a) Ge, Y.; Miller, L.; Ouimet, T.; Smith, D. K. *J. Org. Chem.* **2000**, *65*, 8831. (b) Ge, Y.; Lilienthal, R. R.; Smith, D. K. *J. Am. Chem. Soc.* **1996**, *118*, 3976. (c) Tucker, J. H. R.; Collinson. *Chem. Soc. Rev.* **2002**, *31*, 147.
(14) Kaifer, A. E.; Gómez-Kaifer, M. *Supramolecular Electrochemistry*; Wiley-VCH: Weinheim, Germany, 1999.
(15) (a) Stone, A. J. *The Theory of Intermolecular Forces*; Clarendon Press: Oxford, 1996. (b) Scheiner, S. *Hydrogen Bonding: A Theoretical Perspective*; Oxford University Press: New York, 1997.
(16) See, for example: (a) Kitaura, K.; Morokuma, K. *J. Quantum Chem.* **1976**, *10*, 325−340. (b) Reed, A. E.; Weinhold, F.; Curtiss, L. A.; Pochatko, D. J. *J. Chem. Phys.* **1986**, *84*, 5687−5705. (c) Reed, A. E.; Curtiss, L. A.; Weinhold, F. *Chem. Rev.* **1988**, *88*, 899−926. (d) Weinhold, F. *THEOCHEM-J. Mol. Struct.* **1997**, *399*, 181−197. (e) van der Vaart, A.; Merz, K. M., Jr. *J. Phys. Chem. Soc.* **1999**, *103*, 3321−3329.
(17) See, for example: (a) Buckingham, A. D.; Fowler, P. W.; Hutson, J. M. *Chem. Rev.* **1988**, *88*, 963−988. (b) Singh, U. C.; Kollman, P. A. *J. Am. Chem. Soc.* **1977**, *99*, 4875−4894. (c) Spackman, M. A. *J. Chem. Phys.* **1986**, *85*, 6587−6601.

10.1021/ja035228b CCC: $25.00

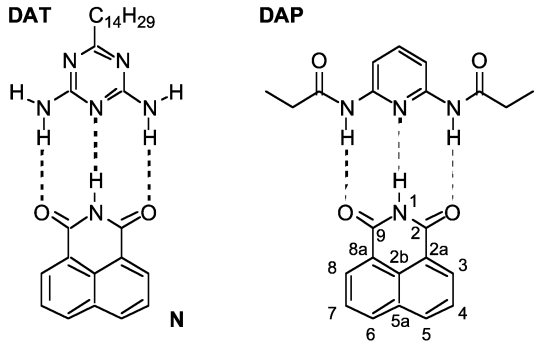

Figure 1. **N·DAT** and **N·DAP** hydrogen-bonded complexes.

important than charge transfer in hydrogen bond formation.[16b] Despite these results, the influence of different hydrogen-bonding energetic components on the reduction properties of electroactive compounds has not been addressed. Understanding the roles each of these components play is an important issue for understanding redox enzymes, as well as having broader implications in multiple areas of biological and supramolecular chemistry. We report here the combined use of spectroscopic and DFT computational techniques to explore the influence of electrostatic and induction events in hydrogen bond formation, as well as upon the electronic consequences of these interactions.

Results and Discussion

(I) Experimental Results. (a) NMR Studies. Previously,[18] we have used electroactive guests to examine spin density redistribution and changes in redox properties upon formation of hydrogen-bonded complexes. In the present study, we model subtle variations in donor−acceptor ability within a three-point hydrogen bond network of interactions upon **N**. To achieve this, we employed two chemically related hosts: diaminotriazine **DAT** and diamidopyridine **DAP** (Figure 1).

Association constants (K_a) for complexes $\mathbf{N_{ox}}$**·DAT** and $\mathbf{N_{ox}}$**·DAP** in the neutral state were determined via ^{1}H NMR titration experiments in CD_2Cl_2, following complexation-induced changes in the chemical shift of the imide proton of $\mathbf{N_{ox}}$.[19] These data were fitted to an appropriate 1:1 binding isotherm applied previously for related systems (Figure 2). Despite the quantitative similarity of the association constants ($K_a\mathbf{N_{ox}}$**·DAT** = 160 ± 10 M^{-1}, $K_a\mathbf{N_{ox}}$**·DAP** = 164 ± 3 M^{-1}), it is worth noting that the ^{1}H NMR limiting value is larger for $\mathbf{N_{ox}}$**·DAT** (δ_{max} = 13.0 ppm) than for $\mathbf{N_{ox}}$**·DAP** (δ_{max} = 12.6 ppm). This suggests a greater basicity associated with the central nitrogen atom in **DAT** as compared to its analogue in **DAP**.[20] Consequently, we may expect the central $N-H_{imide}$- - -$N_{receptor}$ hydrogen bond to be stronger for $\mathbf{N_{ox}}$**·DAT** than for $\mathbf{N_{ox}}$**·DAP**. The data also show that a change in strength of the outer pair of $C{=}O_{imide}$- - -$N-H_{receptor}$ hydrogen bonds compensates completely for the difference in strength of the internal $N-H_{imide}$- - -$N_{receptor}$ interactions, yielding equivalent affinities of the two hosts for $\mathbf{N_{ox}}$.

(b) Electrochemical Studies. Electrochemical generation of radical anions can produce dramatic changes in the electronic distribution without significant rearrangement of molecular structure. We evaluated the ability of each receptor to modulate the redox properties of **N** by quantification of the one-electron

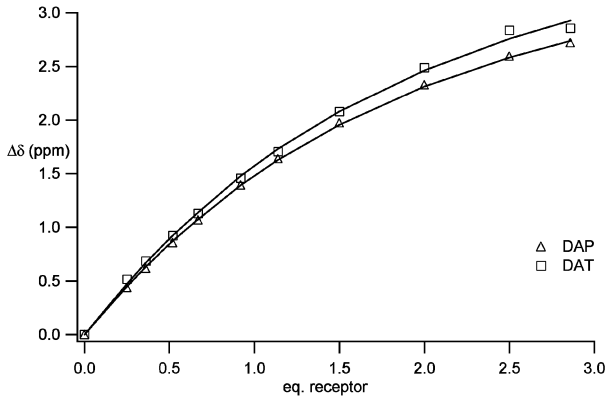

Figure 2. ^{1}H NMR chemical shift of the central N−H imide proton of $\mathbf{N_{ox}}$ vs molar ratio of receptor added. (a) $\mathbf{N_{ox}}$**·DAT** complex K_a = 160 ± 10 M^{-1}, extrapolated limiting chemical shift δ = 13.0 ppm. (b) $\mathbf{N_{ox}}$**·DAP** complex, K_a = 164 ± 3 M^{-1}, extrapolated limiting chemical shift δ = 12.6 ppm.

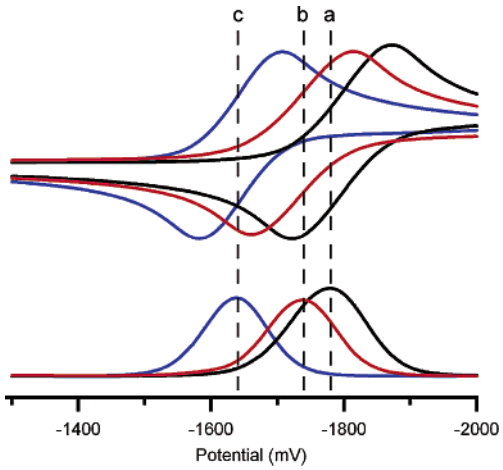

Figure 3. Cyclic (CV) and square wave voltammetric (SWV) plots of (a) **N** alone, (b) **N·DAT**, (c) **N·DAP**. Experiments carried out in CH_2Cl_2 using 0.1 M tetrabutylammonium perchlorate as electrolyte. [**N**] = 1 × 10^{-3} M, receptors added incrementally to saturation. Potentials referenced to ferrocene, used as an internal standard at 23 °C.

electrochemical reduction of bound and unbound naphthalimide to its radical anion in CH_2Cl_2. Our experiments show that receptors **DAT** and **DAP** induce modulation of the reduction of **N** by very different magnitudes (Figure 3). When compared to the unbound guest, binding of receptor **DAP** makes the reduction potential of **N** much less negative (145 mV, 3.3 kcal/mol). This differs significantly from the 44 mV (1.0 kcal/mol) change observed in the formation of complex $\mathbf{N_{red}}$**·DAT**.

Combining the results of the titration experiments with the electrochemical data, summarized in Table 1, allows us to produce redox squares depicting the behavior of the guest with each host (Figure 4). Analysis of the squares makes it apparent that the redox modulation effect is directly related to the affinity of the radical anion form of the host:guest complex, as the other parameters effectively cancel. These results suggest that the electronic structure of the redox active moiety of complex $\mathbf{N_{ox}}$**·DAP** deviates from that of the unbound guest to a much greater extent than in $\mathbf{N_{ox}}$**·DAT**.

(c) EPR Studies. Further experimental insight into the different electronic changes induced by each receptor was obtained through simultaneous electrochemistry and EPR (SEEPR) (Figure 5). Most organic radicals are highly reactive;

(18) Niemz, A.; Rotello, V. M. *J. Am. Chem. Soc.* **1997**, *119*, 6833−6836.
(19) Niemz, A.; Rotello, V. M. *J. Mol. Recognit.* **1996**, *9*, 158−162.
(20) Dunger, A.; Limbach, H.-H.; Weisz, K. *J. Am. Chem. Soc.* **2000**, *122*, 10109−10114.

Table 1. Summary of Energy Changes Associated with DAT and DAP Binding with N

redox label	physical process	experimental data (K_a or $E_{1/2}$)	ΔG (kcal/mol)
ΔG_{1DAT}	$\mathbf{N_{ox}}$+**DAT**- -$\mathbf{N_{ox}}$·**DAT**	160 M^{-1}	−3.0
ΔG_{2DAT}	$\mathbf{N_{ox}}$·**DAT**- -$\mathbf{N_{red}}$·**DAT**	−1738 mV	40.1
ΔG_{3DAT}	$\mathbf{N_{red}}$+**DAT**- -$\mathbf{N_{red}}$·**DAT**	900 M^{-1}	−4.0
ΔG_{4DAT}	$\mathbf{N_{ox}}$+**DAT**- -$\mathbf{N_{red}}$+**DAT**	−1782 mV	41.1
ΔG_{1DAP}	$\mathbf{N_{ox}}$+**DAP**- -$\mathbf{N_{ox}}$·**DAP**	164 M^{-1}	−3.0
ΔG_{2DAP}	$\mathbf{N_{ox}}$·**DAP**- -$\mathbf{N_{red}}$·**DAP**	−1637 mV	37.8
ΔG_{3DAP}	$\mathbf{N_{red}}$+**DAP**- -$\mathbf{N_{red}}$·**DAP**	46 000 M^{-1}	−6.4
ΔG_{4DAP}	$\mathbf{N_{ox}}$+**DAP**- -$\mathbf{N_{red}}$+**DAP**	−1782 mV	41.1

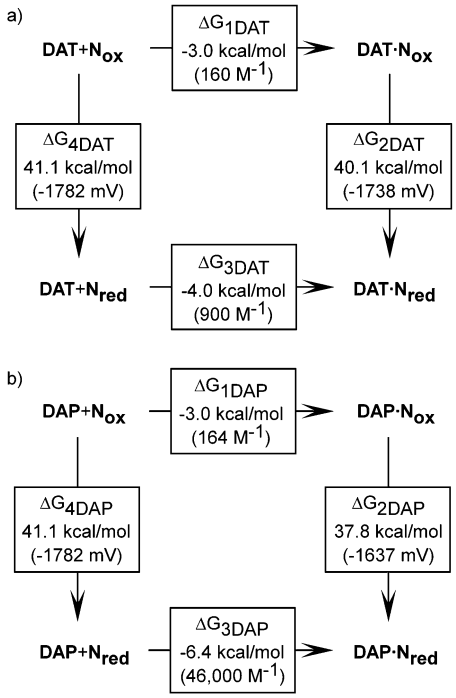

Figure 4. Thermodynamic squares comparing the relative affinities of **N** for **DAT** and **DAP** in both the neutral and the radical anion states. Values corresponding to ΔG_3 processes were obtained according to the relationship $\Delta G_1 + \Delta G_2 + (-\Delta G_3) + (-\Delta G_4) = 0$.

thus standard EPR techniques present some practical difficulties on sample preparation and handling. SEEPR provides the advantage of simultaneous radical generation and spectral acquisition and allows enhanced control of radical concentration. Furthermore, hyperfine coupling constants (hfc's) can be obtained from SEEPR/EPR spectra through standard spectroscopic curve fitting simulation methods.[21]

Hyperfine coupling constants extracted from the SEEPR spectra (Table 2) show that, while both receptors induce changes on the electron spin distribution of $\mathbf{N_{red}}$, the largest quantitative variations occur upon hydrogen bonding with **DAP**, in agreement with the earlier voltammetry results. Association with receptor **DAP** reshapes the electronic distribution of $\mathbf{N_{red}}$ by more than 60% when compared to the changes induced by complexation with **DAT**.

(II) Theoretical Analysis. (a) Energetic Changes Associated with Receptor Binding. To rationalize the experimental data computationally, we performed calculations using the Gaussian suite of programs at the UB3LYP/6-311+G(d,p)//UHF/6-31G(d) level of theory.[22] To simplify the calculations, abridged structures were used (Figure 6). The energy changes associated with the redox squares shown in Figure 3 were reproduced theoretically by examining differences in the total electronic energies on changing state. The results of these calculations are summarized in Table 3 as ΔE_{calc} values. Overall, the results give a good qualitative agreement with the experimental ΔG data as recorded in Table 1.

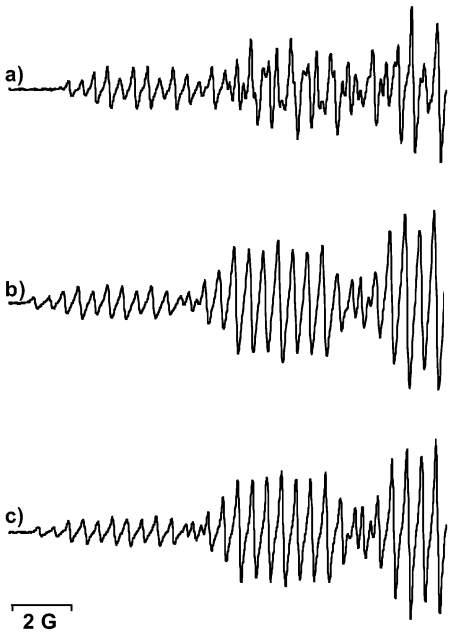

Figure 5. Low field half of the SEEPR spectra of naphthalimide radical anion: (a) 10^{-3} M $\mathbf{N_{red}}$, no receptor, 0.1 M TBAP, degassed, dry CH_2Cl_2. (b) 10^{-3} M $\mathbf{N_{red}}$, 10^{-2} M receptor **DAT**, 0.1 M TBAP, degassed, dry CH_2Cl_2. (c) 10^{-3} M $\mathbf{N_{red}}$, 10^{-2} M receptor **DAP**, 0.1 M TBAP, degassed, dry CH_2Cl_2.

Experimentally, **DAP** and **DAT** were found to have indistinguishable affinities for $\mathbf{N_{ox}}$, with binding favored in each case by 3.0 kcal/mol. The calculations performed for the equivalent gas-phase processes also suggest very similar affinities for the substrate in the oxidized form: ΔE_{calc}($\mathbf{N_{ox}}$+**DAT**- -$\mathbf{N_{ox}}$·**DAT**) = −12.5 kcal/mol, ΔE_{calc}($\mathbf{N_{ox}}$+**DAP**- -$\mathbf{N_{ox}}$·**DAP**) = −10.7 kcal/mol. These values are consistent to within 15%, which is acceptable if one considers that the calculations do not explicitly account for entropic effects or subtle energy differences that may occur due to desolvation of the interacting species. The calculations also correlate strongly with electrochemical data in that binding with **DAP** (for $\mathbf{N_{red}}$+**DAP**- -$\mathbf{N_{red}}$·**DAP**, ΔG_{exp} = −6.4 kcal/mol, ΔE_{calc} = −24.3 kcal/mol) is strongly favored over binding to **DAT** (for $\mathbf{N_{red}}$+**DAT**- -$\mathbf{N_{red}}$·**DAT**, ΔG_{exp} = −4.0 kcal/mol, ΔE_{calc} = −18.4 kcal/mol) when the substrate is present in the radical anion form.

(21) NIEHS WinSim EPR, Duling, D., Laboratory of Molecular Biophysics, NIEHS, NIH, DHHS, 1994.

(22) Frisch, M. J.; Trucks, G. W.; Schlegel, H. B.; Scuseria, G. E.; Robb, M. A.; Cheeseman, J. R.; Zakrzewski, V. G.; Montgomery, J. A., Jr.; Stratmann, R. E.; Burant, J. C.; Dapprich, S.; Millam, J. M.; Daniels, A. D.; Kudin, K. N.; Strain, M. C.; Farkas, O.; Tomasi, J.; Barone, V.; Cossi, M.; Cammi, R.; Mennucci, B.; Pomelli, C.; Adamo, C.; Clifford, S.; Ochterski, J.; Petersson, G. A.; Ayala, P. Y.; Cui, Q.; Morokuma, K.; Malick, D. K.; Rabuck, A. D.; Raghavachari, K.; Foresman, J. B.; Cioslowski, J.; Ortiz, J. V.; Stefanov, B. B.; Liu, G.; Liashenko, A.; Piskorz, P.; Komaromi, I.; Gomperts, R.; Martin, R. L.; Fox, D. J.; Keith, T.; Al-Laham, M. A.; Peng, C. Y.; Nanayakkara, A.; Gonzalez, C.; Challacombe, M.; Gill, P. M. W.; Johnson, B. G.; Chen, W.; Wong, M. W.; Andres, J. L.; Head-Gordon, M.; Replogle, E. S.; Pople, J. A. *Gaussian 98*, revision A.9; Gaussian, Inc.: Pittsburgh, PA, 1998.

Table 2. Experimental and Calculated hfc's (G) for $\mathbf{N_{red}}$, $\mathbf{N_{red}}$**·DAT**, and $\mathbf{N_{red}}$**·DAP**

	experimental					B3LYP/6-311+G(d,p)//HF/6-31G(d)				
atom	$\mathbf{N_{red}}$	$\mathbf{N_{red}}$**·DAT**	$(\Delta_{hfc})^a$	$\mathbf{N_{red}}$**·DAP**	$(\Delta_{hfc})^a$	$\mathbf{N_{red}}$	$\mathbf{N_{red}}$**·DAT**	$(\Delta_{hfc})^a$	$\mathbf{N_{red}}$**·DAP**	$(\Delta_{hfc})^a$
N(1)	0.483	0.530	(0.047)	0.533	(0.050)	0.442	0.535	(0.093)	0.554	(0.112)
H(1)	1.414	1.470	(0.048)	1.492	(0.078)	1.041	1.103	(0.062)	1.153	(0.112)
H(3)/H(8)	5.092	5.210	(0.049)	5.282	(0.190)	4.490	4.763	(0.273)	4.974	(0.484)
H(4)/H(7)	0.901	0.990	(0.050)	1.028	(0.127)	0.758	0.969	(0.211)	1.114	(0.356)
H(5)/H(6)	5.729	5.740	(0.051)	5.763	(0.034)	5.917	5.961	(0.044)	6.029	(0.112)

[a] $\Delta_{hfc} = |hfc(\mathbf{N_{red}}\cdot\mathbf{receptor})| - |hfc(\mathbf{N_{red}})|$.

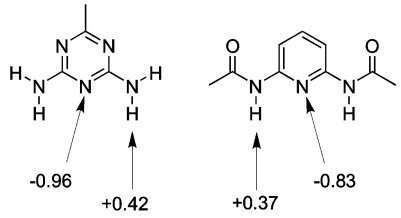

Figure 6. Abridged DAT and DAP structures with UB3LYP/6-311+G-(d,p)//UHF/6-31G(d) Merz−Singh−Kollman calculated atomic charges for the recognition contacts of isolated hosts **DAT** and **DAP**.

Table 3. Summary of Calculated Energy Changes Associated with **DAT** and **DAP** Binding with **N**

physical process (**DAT**)	ΔE_{calc} (kcal/mol)[a]	physical process (**DAP**)	ΔE_{calc} (kcal/mol)[a]
$\mathbf{N_{ox}}$**+DAT- -$\mathbf{N_{ox}}$·DAT**	−12.5	$\mathbf{N_{ox}}$**+DAP- -$\mathbf{N_{ox}}$·DAP**	−10.7
$\mathbf{N_{ox}}$**·DAT- -$\mathbf{N_{red}}$·DAT**	−44.0	$\mathbf{N_{ox}}$**·DAP- -$\mathbf{N_{red}}$·DAP**	−51.7
$\mathbf{N_{red}}$**+DAT- -$\mathbf{N_{red}}$·DAT**	−18.4	$\mathbf{N_{red}}$**+DAP- -$\mathbf{N_{red}}$·DAP**	−24.3
$\mathbf{N_{ox}}$**+DAT- -$\mathbf{N_{red}}$+DAT**	−38.1	$\mathbf{N_{ox}}$**+DAP- -$\mathbf{N_{red}}$+DAP**	−38.1

[a] ΔE_{calc} values from calculations performed at the UB3LYP/6-311+G(d,p)//UHF/6-31G(d) level of theory.

The electrochemical data can also be compared to calculated energy changes in a similar manner. To make the experimental data more directly comparable with energy values obtained through the computational methods, it is easier to transpose the data to $\Delta\Delta G$ and $\Delta\Delta E$ values, where these values correspond to changes in energy due to complexation canceling as many effects as possible.[23] Experimentally, it was shown that **DAT** brought about a modest cathodic shift in the reduction potential $\Delta E_{1/2} = 44$ mV, equivalent to a $\Delta\Delta G_{exp} = -1.0$ kcal/mol, with a $\Delta\Delta E_{calc} = -5.9$ kcal/mol being predicted theoretically. The **DAP** based receptor was shown to bring about a much greater cathodic shift in the reduction potential of naphthalimide, $\Delta E_{1/2} = 145$ mV, giving a $\Delta\Delta G_{exp} = -3.3$ kcal/mol; a $\Delta\Delta E_{calc} = -13.6$ kcal/mol was predicted theoretically. Overall, this series of calculations shows a qualitative agreement with the experimental findings in that the two receptors bind the same electroactive substrate with equal affinity in one oxidation state while displaying significant differences in binding to the same substrate in a second oxidation state coupled with substantial differences in redox modulation effects.

(b) Electrostatic Components of Receptor Binding. The NMR results were validated by examination of the theoretical shielding tensor of the imide proton of **N** in both complexes. The results of the calculations agree well with the experimental findings in that resonance occurs further downfield in the DAT complex (δ_{max}calc = 12.2 ppm, δ_{max}exp = 13.0 ppm) than in the DAP containing complex (δ_{max}calc = 11.0 ppm, δ_{max}exp = 12.6 ppm). This effect could be attributed to a stronger electrostatic potential associated with the N(1) atom of **DAT** in comparison to **DAP**.

Electrostatic potential-derived atomic charges for the isolated receptors were calculated using the Merz−Singh−Kollman approach.[24] Atomic charges (Figure 6) show the central nitrogen of the **DAT** recognition unit to be more basic (negatively charged) than its counterpart in the **DAP** system, in excellent agreement with the limiting chemical shift values obtained from ^{1}H NMR experiments (vide supra). In addition, the calculations show the amine protons of **DAT** to be more electrostatically positive than the amide protons of **DAP**. This indicates that the electrostatic component of the binding energy is greater in the **N·DAT** systems than the **N·DAP** counterparts. As both receptors have equal affinity for the guest, energetic components from other sources such as induction effects must play a more pronounced role in the **N·DAP** binding process.

(c) Geometric Changes Associated with Receptor Binding. An examination of the calculated geometry changes associated with the binding and reduction processes reveals further important information regarding the nature of the interaction between the two host−guest systems (Table 4). The binding process between $\mathbf{N_{ox}}$ and the two receptors induces a small lengthening of the amine N−H bonds of **DAT** and likewise a similar lengthening of the amide N−H bonds of **DAP**. This change in bond length is normal in most hydrogen-bonded systems and correlates directly with the often observed red-shift in the IR spectrum.[11b] The imide N−H of $\mathbf{N_{ox}}$ also lengthens upon binding with both **DAP** and **DAT**; however, the magnitude of the change with the latter receptor is greater, again suggesting that this bond is stronger in **DAT·**$\mathbf{N_{ox}}$ than in **DAP·**$\mathbf{N_{ox}}$. The carbonyl groups of $\mathbf{N_{ox}}$ also lengthen on binding; however, this effect is both small and nearly identical upon binding with either receptor.

Reduction of the bound complexes to the corresponding radical anions induces further more substantial changes in the binding site geometries. First, the outer hydrogen bonds between the carbonyl oxygen atoms of **N** and the amine/amide protons of the receptors shorten dramatically upon reduction to the radical anion. The contraction when **DAP** is bound to **N** is, however, substantially greater than when **DAT** is employed (0.165 vs 0.130 Å). Second, a further lengthening of the amine and amide N−H groups of **DAT** and **DAP** occurs (0.010 Å each), in line with the greater hydrogen-bond-donating properties of the carbonyl groups of $\mathbf{N_{red}}$ over $\mathbf{N_{ox}}$. Also, in each case, the carbonyl groups of **N** lengthen upon reduction; however, there is only a slight difference in this expansion according to which receptor is used.

(23) That is, from the redox cycles depicted in Figure 3, $\Delta\Delta G_{exp}(DAT) = \Delta G_{2DAT} - \Delta G_{4DAT}$, etc.

(24) (a) Besler, B. H.; Merz, K. M.; Kollman, P. A. *J. Comput. Chem.* **1990**, *11*, 431. (b) Singh, U. C.; Kollman, P. A. *J. Comput. Chem.* **1984**, *5*, 129. (c) Implemented within the Gaussian suite of programs using: Glendening, E. D.; Reed, A. E.; Carpenter, J. E.; Weinhold, F. NBO Version 3.1.

Table 4. Selected Bond Length Data from Calculated Geometries (Å)

bond	**DAT**+$\mathbf{N_{ox}}$	**DAT**·$\mathbf{N_{ox}}$	($\Delta_{binding}$)[a]	**DAT**·$\mathbf{N_{red}}$	($\Delta_{reduction}$)[b]	**DAP**+$\mathbf{N_{ox}}$	**DAP**·$\mathbf{N_{ox}}$	($\Delta_{binding}$)[c]	**DAP**·$\mathbf{N_{red}}$	($\Delta_{reduction}$)[d]
N−$H_{DAP/DAT}$	0.993	0.998	0.005	1.008	0.010	0.996	0.999	0.003	1.009	0.010
N−H_N	0.999	1.013	0.014	1.004	−0.009	0.999	1.009	0.009	1.002	−0.006
C═O_N	1.195	1.201	0.006	1.235	0.034	1.195	1.201	0.006	1.237	0.036
O_N···$H_{DAP/DAT}$		2.100		1.970	−0.130		2.115		1.950	−0.165
$N_{DAP/DAT}$···H_N		2.065		2.067	0.002		2.279		2.230	−0.049
O_N···H−$N_{DAP/DAT}$		3.096		2.978	−0.117		3.094		2.937	−0.157
$N_{DAP/DAT}$···H−N_N		3.078		3.071	−0.007		3.288	-	3.233	−0.055

[a] $\Delta_{binding}$ = length(**DAT**·$\mathbf{N_{ox}}$) − length(**DAT**+$\mathbf{N_{ox}}$). [b] $\Delta_{reduction}$ = length(**DAT**·$\mathbf{N_{red}}$) − length(**DAT**·$\mathbf{N_{ox}}$). [c] $\Delta_{binding}$ = length(**DAP**·$\mathbf{N_{ox}}$) − length(**DAP**+$\mathbf{N_{ox}}$). [d] $\Delta_{reduction}$ = length(**DAP**·$\mathbf{N_{red}}$) − length(**DAP**·$\mathbf{N_{ox}}$).

Finally, changes in geometry also occur within the atoms comprising the central hydrogen bond of each system. The hydrogen bond itself is relatively unchanged upon reduction for the **DAT** triazine system (lengthens by 0.002 Å); however, a significant shortening is observed when bound to **DAP** (0.049 Å). In addition, the imide bond of **N** undergoes a small contraction when bound to either receptor with the change slightly greater in the presence of **DAT** (0.009 Å) than **DAP** (0.006 Å). Two factors may contribute to this observation: (i) the addition of an extra electron to naphthalimide increases the electron density associated with the imide nitrogen, which in turn would pull the electron-deficient proton closer electrostatically; (ii) the dramatic contraction between the two interacting partners associated with strengthening the outer hydrogen bonds may cause an unfavorable interpenetration of the van der Waals radii at the central hydrogen bond contact that could be alleviated by a shortening of the imide bond.

(d) HFC and Spin Density Analysis. The fitted hfc data (Table 2) can also be directly compared with computationally derived values obtained from the theoretical calculations, providing a two-way validation tool. Overall, the fitted and calculated hfc values show excellent agreement, with a 5% RMS difference between calculated and fitted data sets. The trends in the differences between hfc measurements of complexed and noncomplexed naphthalimide were also reproduced theoretically. Upon complexation with either guest, the hfc corresponding to every atom measured in naphthalimide was found to increase, indicating greater overall spin polarization with the largest effects being exhibited within the naphthalene moiety of **N**. Furthermore, every hfc value for $\mathbf{N_{red}}$·**DAP** increased to a greater extent than $\mathbf{N_{red}}$·**DAT**. The computational results agree fully with the experimental findings.

The excellent agreement between the theoretical treatment and experimental data permits us to examine related molecular properties that are not readily probed experimentally, such as changes in the spin density of these systems. Quantification of the differences in spin density between the bound and unbound radical anion shows that again the larger changes are seen when $\mathbf{N_{red}}$ is bound to **DAP** (Table 5). These changes are manifested as a shift in spin away from the imide unit and into the naphthyl ring system. The rationalization of this behavior lies in the fact that hydrogen bonding takes place via pairs of electrons from filled orbitals. Upon binding to the receptors, a distortion in these orbitals can take place through an induction mechanism such that greater electron density resides near the carbonyl oxygens. As a result of this behavior, the semioccupied molecular orbital (SOMO) containing the unpaired electron of the radical anion becomes distorted in the opposite direction to compensate for the shift in electron density. From this rationalization, it is apparent that the **DAP** receptor causes a greater induction effect than **DAT**, with a concomitant higher energetic component from this effect stabilizing the resulting complex.[19]

Table 5. Calculated Spin Densities (sd)

atom	$\mathbf{N_{red}}$	$\mathbf{N_{red}}$·**DAT**	Δ[a]	$\mathbf{N_{red}}$·**DAP**	Δ[a]
N(1)	−0.032	−0.037	0.005	−0.035	0.003
C(2)/C(9)	0.062	0.075	0.013	0.078	0.016
O(2)/O(9)	0.076	0.077	0.001	0.075	−0.001
C(2a)/C(8a)	0.030	0.003	−0.027	0.010	−0.020
C(3)/C(8)	0.215	0.228	0.013	0.240	0.025
C(4)/C(7)	0.066	−0.075	0.009	−0.086	0.020
C(5)/C(6)	0.304	0.312	0.008	0.301	−0.003
C(5a)	−0.104	−0.095	−0.009	−0.101	−0.003
C(2b)	−0.052	−0.050	−0.002	−0.044	−0.008

[a] Difference in absolute magnitudes: Δ = |sd(**$\mathbf{N_{red}}$·receptor**)| − |sd(**$\mathbf{N_{red}}$**|.

Electrostatic potential slices obtained from the calculations (Figure 7) provide the most striking evidence for the differences in the relative contributions of electrostatic and induction events in guest binding. From these pictures, we can clearly see that the electrostatic potential surface over N(1) for the **DAT** receptor must be more negative than that of the corresponding position in **DAP**, again evidence of the enhanced basicity of that position in **DAT**. Moreover, the electrostatic potential maps also provide information about the relative importance of induction processes during hydrogen bond formation. In case of the $\mathbf{N_{ox}}$·**DAP** host−guest pair, the electronic cloud of the N−H group in **DAP** is strongly deformed (polarized) toward the naphthalimide guest upon hydrogen bonding, as seen by the intermingling of the potential surfaces at these positions. At the N(1) position, the distinct separation of the electronic structures of host and guest can clearly be seen, indicating a predominantly electrostatic contact at this position. Electrostatic effects are predominant throughout the three contacts between the **DAT** and **N** as seen by the complete separation of the electronic structures of the host−guest pair.

Similar electrostatic slices obtained for the corresponding radical anionic complexes show similar trends in the electronic differences induced by the two complexes (Figure 8). Again, in both complexes, distinct separation occurs at the region between the N1 position of the receptor and the imide proton of the substrate, indicative of a predominantly electrostatic contact. Moreover, the electronic nature of the outer hydrogen bonds in the reduced complexes also parallels those displayed by their oxidized counterparts. Predominantly electrostatic contacts are once more present between the amine protons of **DAT** and the carbonyl oxygens of $\mathbf{N_{red}}$, whereas the corresponding positions in **DAP**·$\mathbf{N_{red}}$ again have a more pronounced polarization component. Taken as a whole, the results of this investigation indicate that, although electrostatic contacts act to provide effective binding between host and guest, it is the

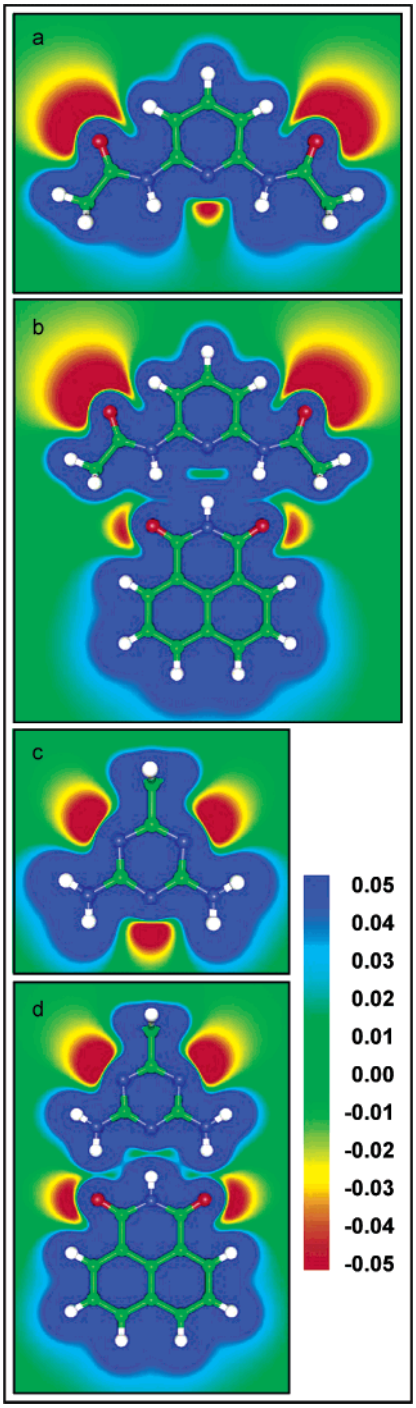

Figure 7. Electrostatic potential slices calculated at the B3LYP/6-311+G-(d,p)//UHF/6-31G(d) level for the neutral receptors (a) **DAP**, (c) **DAT** and complexes (b) $\mathbf{N_{ox}}$·**DAP**, (d) $\mathbf{N_{ox}}$·**DAT**. The scale bar indicates the magnitude of the electrostatic potential in hartrees.

often overlooked induction component of the binding energy which is more important in controlling electronic properties.

Conclusions

In summary, we have used a combination of theoretical calculations and spectroscopic techniques to investigate two distinctive driving forces in hydrogen bond formation, which compete in two chemically related receptors. Despite sharing similar association constants, the $\mathbf{N_{ox}}$·**DAT** and $\mathbf{N_{ox}}$·**DAP** complexes are formed due to very different driving forces. The

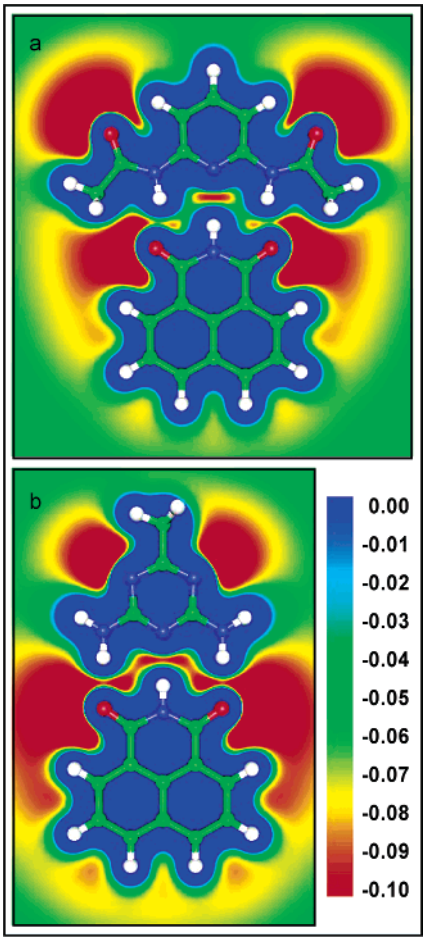

Figure 8. Electrostatic potential slices calculated at the B3LYP/6-311+G-(d,p)//UHF/6-31G(d) level for the complexes (a) $\mathbf{N_{red}}$·**DAP**, (b) $\mathbf{N_{red}}$·**DAT**. The scale bar indicates the magnitude of the electrostatic potential in hartrees.

recognition process for $\mathbf{N_{ox}}$·**DAT** is mainly driven by electrostatic interactions between the imide unit of $\mathbf{N_{ox}}$ and complementary contacts of **DAT**. In contrast, formation of the $\mathbf{N_{ox}}$·**DAP** complex is directed by a facilitated polarization of the external N−H bonds on the **DAP** component toward the naphthalimide carbonyls. The two different hydrogen-bonding events compensate for each other almost perfectly in the neutral complexes, producing the similarity in association constants measured. Both recognition processes, electrostatic interaction and induction, have very different effects on the electronic density redistribution of the electroactive guest **N**, generating the differences observed in the SEEPR spectra and electrochemical behavior.

Currently, we are actively applying the results of this investigation to rationally design improved host systems for biomimetic experiments and electroactive devices. We will disclose the results of our subsequent investigations in due course.

Experimental Section

Materials and General Methods. Solutions utilized in electrochemical and SEEPR experiments were prepared using reagent grade CH_2Cl_2 dried via distillation over CaH_2. Tetrabutylammonium perchlorate (TBAP, obtained from SACHEM, electrometric grade) was dissolved in $CHCl_3$, washed with distilled water, recrystallized twice from ethyl acetate, and dried for several days under high vacuum.

Naphthalimide (obtained from Aldrich Chemical Co.) was crystallized from a $CHCl_3$:EtOH (1:1) mixture and dried under high vacuum. Other chemicals were reagent grade, obtained from Aldrich, and used without further purification. The syntheses of both **DAP** and **DAT** have been previously described.

Determination of Association Constants for 1·2 and 1·3 Complexes by ^{1}H NMR Titration.[25] These experiments were performed in a noncompetitive solvent under constant concentration conditions of **N** at 298 K. **N** stock solution ($CDCl_3$ solvent; 2 mL, 0.99 mg mL^{-1}, 5 mM) was used to prepare 20 mM solutions of the receptor molecules (**DAP** = 8.85 mg, **DAT** = 12.29 mg). A further 600 μL of the stock solution was transferred to an NMR tube, and the spectrum of this solution was recorded in a Brucker AC200 200 MHz NMR spectrometer. Aliquots of the receptor solution were added, with spectra recorded for each addition, and the incremental downfield change in the chemical shift of the naphthalimide imide resonance was noted.

The resulting data were analyzed to reveal the binding constant K_a by application of nonlinear least-squares curve fitting.[26] The data for each curve gave excellent agreement with the 1:1 binding isotherm, using the relationship

$$\partial_{obs} = \partial_H + \frac{(\partial_{HG} - \partial_H)\left(\left([H_t] + [G_t] + \frac{1}{K_a}\right) - \left(\left([H_t] + [G_t] + \frac{1}{K_a}\right)^2 - 4[H_t][G_t]\right)^{1/2}\right)}{2[H_t]}$$

where $[G_t]$ and $[H_t]$ correspond, respectively, to the total concentrations of guest and host, δ_{obs} is the observed chemical shift, δ_H represents the chemical shift of the imide proton of the host in the absence of guest, and δ_{HG} is the chemical shift of the followed proton in the fully bound complex, estimated from extrapolation from the limiting experimental value.[27]

Electrochemistry. All electrochemical experiments were carried out on a Cypress System potentiostat. A 1 mm platinum button and a gold-plated electrode were utilized as working and reference electrodes, respectively. A silver wire pseudo reference electrode was used, and all potentials are referenced versus the ferrocene/ferrocenium couple. The sweep rate was 350 mV/s, and the studies were run on an argon-purged temperature-controlled cell. Solutions of **N**, **DAT·N**, and **DAP·N** were prepared maintaining a constant concentration of **N**, with the receptors added to saturation. The solutions were degassed by bubbling argon through them for at least 10 min, at which time cyclic and square wave voltammograms were recorded (for representative voltammograms, see Supporting Information).

Simultaneous Electrochemistry and EPR. To minimize perturbation of the microwave field by the working electrode, SEEPR experiments were carried out in a quartz flat cell. A second glass part containing three ACE no. 7 threaded joints sealed via Teflon ferrules to hold the electrodes and a septum-capped ground glass joint for degassing and sample injection was connected to the top of the cell. The working electrode, a platinum gauze electrode, was inserted into the flat part of the cell. The Ag-wire pseudo reference electrode was positioned directly above the working electrode to minimize the iR-drop, and the auxiliary electrode, a platinum wire spiral of large surface area, occupied the solvent reservoir above the flat section.

EPR spectra were recorded on an IBM ESP 300 X-band spectrometer equipped with a TE_{104} dual cavity. Solutions were prepared following the same procedure as for electrochemical studies. They were then injected into the cell, which was previously flushed with argon. The cell was mounted within the spectrometer using custom manufactured cell holders, which allow for precise alignment of the cell within the cavity to maximize the Q-factor. Electrolysis and signal acquisition were carried out simultaneously (25 kHz field modulation, modulation amplitude 0.0475 G). Hyperfine coupling constants were determined through spectrum simulation and iterative curve-fitting using the software package WinSim from NIEHS.[21] Excellent correlation ($r^2 > 0.99$) was achieved in all cases.

Calculations. HF and B3LYP calculations were performed using the Gaussian 98W suite of programs.[22] Geometry optimizations were run at the UHF/6-31G(d) level, followed by frequency calculations at the same level, and then UB3LYP/6-311+G(d,p) single point calculations. To increase calculation speed, the *n*-tetradecane aliphatic chain present in triazine receptor **DAT** was replaced by a methyl group, while the two propanoyl groups on receptor **DAP** were replaced by acetyl groups. All calculations were performed without applying correction for basis set superposition error (BSSE). In addition to the considerable increase in computer time, the implementation of BSSE corrections is expected to almost completely cancel out between the two hydrogen-bound complexes. Isotropic hfc's are explicitly provided by Gaussian 98, allowing direct comparison of theoretical values with those obtained experimentally (for further details on the theoretical investigation, see Supporting Information).

Acknowledgment. This research was supported by the National Institutes of Health (GM59249) and the National Science Foundation (CHE-0213354). The authors would like to thank Peter Bryngelson and Justin Fermann of the Department of Chemistry at the University of Massachusetts Amherst for helpful discussions.

Supporting Information Available: ^{1}H NMR titration data, cyclic voltammetry and square wave voltammetry plots for **N**, **N·DAT**, and **N·DAP**, and calculation details including optimized geometries (PDF). This material is available free of charge via the Internet at http://pubs.acs.org.

JA035228B

(25) Previous experimental results have demonstrated that receptors **2** and **3** do not dimerize or aggregate under the experimental conditions used in our study.

(26) Long, J. R.; Drago, R. S. *J. Chem. Soc.* **1982**, *59*, 1037−1039.
(27) For further information, see: Conners, K. *Binding Constants*; Wiley and Sons: New York, 1987.